

A Quantum Mechanics Analogy for the Nonlinear Schrödinger Equation in the Finite Line

J. I. Ramos and F. R. Villatoro
Departamento de Lenguajes y Ciencias de la Computación
E. T. S. Ingenieros Industriales
Universidad de Málaga
Plaza El Ejido, s/n
29013-Málaga
SPAIN

Abstract

A quantum mechanics analogy is used to determine the forces acting on and the energies of solitons governed by the nonlinear Schrödinger equation in finite intervals with periodic and with homogeneous Dirichlet, Neumann and Robin boundary conditions. It is shown that the energy densities remain nearly constant for periodic, while they undergo large variations for homogeneous, boundary conditions. The largest variations in the force and energy densities occur for the Neumann boundary conditions, but, for all the boundary conditions considered in this paper, the magnitudes of these forces and energies recover their values prior to the interaction of the soliton with the

boundary, after the soliton rebound process is completed. It is also shown that the quantum momentum changes sign but recovers its original value after the collision of the soliton with the boundaries. The asymmetry of the Robin boundary conditions shows different dynamic behaviour at the left and right boundaries of the finite interval.

KEYWORDS: Nonlinear Schrödinger equation, two-point initial-value problems, quantum analogy, forces

1 Introduction

The one-dimensional nonlinear Schrödinger equation is ubiquitous in many branches of mathematics, physics and engineering [1] and [2], e.g., fluid mechanics, plasma physics, nonlinear optics, nonlinear wave propagation, etc. Its initial-value problem is integrable by the inverse scattering transform and has a truly remarkable analytical structure. Despite the great interest that this equation has received in the past two decades through analytical and numerical studies, the existence and uniqueness of the nonlinear Schrödinger equation in the quarterplane, i.e., for semi-infinite spatial domains, seems to remain an issue of current research [3].

Three main lines of research on the nonlinear Schrödinger equation in the quarterplane have been undertaken. The first is based on results obtained numerically and uses ad hoc assumptions [4]. The second one is based on the use of the inverse scattering transform and Bäcklund transformations [5], while the third one employs the infinite sine Fourier transform [6]. However,

these three lines of research have been concerned with the generation of solitons at the boundaries, e.g., boundary-generated solitons.

Ablowitz and Segur [7] showed that the quarter-plane, initial-boundary value problem is solvable by means of the nonlinear, sine Fourier transform if certain symmetry conditions hold. In particular, Ablowitz and Segur [7] proved the solvability of semi-infinite line problems subject to homogeneous Dirichlet or Neumann conditions. Fokas [6] and Bikbaev and Tarasov [5] have extended this result to semi-infinite line problems subject to homogeneous Robin boundary conditions. Fokas [6] has studied the generation of solitons by a non-homogeneous Robin boundary condition in the semi-infinite line with zero initial conditions.

Some authors believe in the almost integrability of the nonlinear Schrödinger equation in the quarterplane, also called ‘forced integrable nonlinear Schrödinger equation’ [9] because the boundary conditions can be viewed as forces that act at the boundaries. Kaup [9] showed that the difficulty in the solvability of the forced Dirichlet initial-boundary value problem in the quarterplane lies in the determination of the spatial derivative of the amplitude at the boundary, and in the determination of its primitive in the Neumann case. However, his studies have not been able to provide a connection, if there is any, between solitons in initial-value and quarterplane problems. Other authors, such as Kaup [8] and Kaup and Hansen [4] have studied both analytically and numerically the generation of solitons in quarter-plane problems subject to non-homogeneous Dirichlet boundary conditions.

If little is known about the existence and uniqueness of solutions of the nonlinear Schrödinger equation in the quarterplane, much less is known about

that equation in finite intervals, i.e., two-point, initial-boundary value problems, because neither the inverse scattering transform nor the infinite sine Fourier transform can be applied to them. Numerical solutions, however, may be obtained for these problems by employing, for example, global spectral, finite difference or finite element methods. In this paper, a numerical study of the nonlinear Schrödinger equation subject to periodic and to homogeneous Dirichlet, Neumann and Robin boundary conditions in finite intervals is presented in order to determine the forces on and the energies of the solitons by using a quantum mechanics analogy. An analogy similar to the one presented in this paper has been previously used by Bian and Chan [10] who only studied the nonlinear and diffraction forces on solitons governed by the initial-value problem of the nonlinear Schrödinger equation. These authors, however, used a filter and their force and energy densities are not consistent with a strict quantum mechanics analogy.

2 The One-Dimensional, Nonlinear Schrödinger Equation

The one-dimensional, time-dependent, nonlinear Schrödinger equation with a cubic potential can be written as

$$i\hbar \hat{u}_t = -\frac{\hbar^2}{2m}\hat{u}_{xx} + V\hat{u} \quad (1)$$

where the potential well has the following form

$$V = -q\frac{\hbar^2}{m}|\hat{u}|^2 \quad (2)$$

\hat{t} is time, \hat{x} is the spatial coordinate, \hat{u} is a complex amplitude, \hbar is the Planck constant, q is a coefficient, m is the mass of the soliton considered as a quantum particle, and the subscripts denote partial differentiation.

A quantum-like analog of the nonlinear Schrödinger equation can be easily obtained by assuming that the complex amplitude, \hat{u} , of the nonlinear Schrödinger equation is like the wave function of a quantum particle. This allows to determine its quantum momentum, quantum energy and forces as follows. The linear quantum momentum is defined by the one-dimensional operator [11]

$$\hat{P} \equiv -i\hbar \frac{\partial}{\partial \hat{x}} \quad (3)$$

whose mean value is given by the following time-dependent expression

$$\langle P \rangle = \frac{\langle \hat{u}, \hat{P}\hat{u} \rangle}{\langle \hat{u}, \hat{u} \rangle} = -i\hbar \frac{\int_{\mathcal{D}} \hat{u}^* \hat{u}_x d\hat{x}}{\int_{\mathcal{D}} \hat{u}^* \hat{u} d\hat{x}} \quad (4)$$

where \mathcal{D} is the spatial domain, and \hat{u}^* denotes the complex conjugate of \hat{u} .

The quantum momentum density may be defined as

$$p(\hat{x}, \hat{t}) = -i\hbar \hat{u}^* \hat{u}_x. \quad (5)$$

The linear quantum energy is defined by the operator

$$\hat{E} = i\hbar \frac{\partial}{\partial \hat{t}} \quad (6)$$

whose mean value is

$$\langle E \rangle = \frac{\langle \hat{u}, \hat{E}\hat{u} \rangle}{\langle \hat{u}, \hat{u} \rangle} = i\hbar \frac{\int_{\mathcal{D}} \hat{u}^* \hat{u}_t d\hat{x}}{\int_{\mathcal{D}} \hat{u}^* \hat{u} d\hat{x}}. \quad (7)$$

The energy density is

$$e(\hat{x}, \hat{t}) = i\hbar \hat{u}^* \hat{u}_t. \quad (8)$$

Equation (1) can be nondimensionalized using the linear transformations

$$\hat{u} \rightarrow \sqrt{\frac{m}{q\hbar}}u, \quad \hat{t} \rightarrow t, \quad \hat{x} \rightarrow \sqrt{\frac{\hbar}{2m}}x \quad (9)$$

to yield

$$iu_t = -u_{xx} - |u|^2u \quad (10)$$

Hereon, unless otherwise stated, nondimensional variables will be used. Note that the above dimensional definitions of the quantum momentum and energy may be used to obtain their dimensionless counterparts by simply setting \hbar and m equal to unity in the definitions of the dimensional quantum momentum and energy densities.

The energy density can be written as

$$e(x, t) = -(u^*u_{xx} + |u|^4) = e_k(x, t) + e_v(x, t) \quad (11)$$

where the kinetic and potential energy densities are, respectively,

$$e_k(x, t) = -u^*u_{xx}, \quad e_v(x, t) = -|u|^4. \quad (12)$$

The spatial derivatives of the energy densities define effective force densities as follows. From the potential energy density, the following nonlinear force density that produces self-focusing on solitons is obtained

$$f_n(x, t) = -\frac{\partial}{\partial x}e_v(x, t) = \frac{\partial}{\partial x}(|u|^4) \quad (13)$$

while, from the kinetic one, the following diffraction force density that is responsible for the diffraction effect on the soliton results

$$f_d(x, t) = -\frac{\partial}{\partial x}e_k(x, t) = \frac{\partial}{\partial x}(u^*u_{xx}). \quad (14)$$

The kinetic energy and diffraction force densities defined above have complex values. In quantum mechanics, only the mean values of the energy and force can be physically measured and these values are always real due to the Hermitian quantum operators.

In order to obtain physical insight from the energy and force densities defined above, it is convenient to use real values by taking either their real or imaginary part. In this paper, the real parts of the energy and force densities are used.

A physically and mathematically consistent use of the quantum analogy may also be obtained by defining the energy density as e/ϱ where ϱ is a constant. For example, the following renormalization factor may be used for the initial value problem of the nonlinear Schrödinger equation

$$\varrho = \int_{\mathcal{D}} u^* u dx \quad (15)$$

which coincides with the first invariant of the initial-value problem of the nonlinear Schrödinger equation. However, this value of ϱ may not be constant for two-point, initial-boundary-value problems (cf. Section 4), i.e., it may not be used to obtain a physically and mathematically consistent quantum analogy for two-point, initial value problems.

Bian and Chan [10] defined the energy density as e/ϱ where $\varrho=u^*u$ in order to assess physically that a soliton can be considered as the result of two opposite phenomena, i.e., the diffraction and the self-focusing caused by dispersion and nonlinearity, respectively, for the initial-value problem of Eq. (10). Since their renormalization factor, ϱ , is a function of both space and time, its use is not consistent with a quantum mechanics analogy for the nonlinear Schrödinger equation. As a consequence, the energy and force

densities obtained by Bian and Chan are somewhat artificial, since their filter or renormalization factor affects the values of these densities in a different manner depending on the soliton location at each instant of time.

The 1-soliton solution of the initial-value problem for Eq. (10) is

$$u(x, t) = A \operatorname{sech}(\xi) \exp(i\eta). \quad (16)$$

where

$$\xi = \frac{A}{\sqrt{2}}(x - x_0 - ct) \quad (17)$$

$$\eta = \frac{1}{2}[c(x - x_0) + (A^2 - \frac{c^2}{2})t + \phi_0], \quad (18)$$

A , c , x_0 and ϕ_0 are the soliton's amplitude, velocity, initial position and initial phase, respectively, and the nonlinear and diffraction force densities for $\varrho=1$ are, respectively,

$$f_n = -2\sqrt{2}A^5 \operatorname{sech}^4\xi \tanh \xi \quad (19)$$

$$f_d = \frac{A^3}{4} \operatorname{sech}^2\xi \left[-6Aci \operatorname{sech}^2\xi + 8\sqrt{2}A^2 \operatorname{sech}^2\xi \tanh \xi + \sqrt{2}(c^2 - 2A^2) \tanh \xi + 4Aci \right] \quad (20)$$

while the total force density, i.e., the sum of the nonlinear and diffraction force densities, is

$$f_t = \frac{A^3}{4} \operatorname{sech}^2\xi \left[-6Aci \operatorname{sech}^2\xi + \sqrt{2}(c^2 - 2A^2) \tanh \xi + 4Aci \right] \quad (21)$$

The above equations show that the nonlinear force density is less than zero behind the location of the soliton's maximum amplitude and greater

than zero in front of it, whereas the real parts of both the diffraction and total force densities depend on the values of c and A .

The numerical results of Bian and Chan [10] indicate that their total force density, i.e., the sum of the real part of the diffraction force and the nonlinear force densities, vanishes for the 1-soliton solution, cf. Eq. (16). For the exact N -soliton solution [13, 14], the energy density of Bian and Chan gives a nonvanishing force dominated by the nonlinear density force which indicates that the solitons are compressed while propagating. However, their interpretation can be criticized on the grounds that diffraction effects on the soliton must also be considered and that their renormalization factor which is a function of both space and time, affects in different manner the local force densities. Furthermore, it is important to note that their definition can cause computational problems when calculating the nonlinear and diffraction force densities due the small denominator introduced by the filter in their energy expression, especially in the soliton tails.

3 Boundary Conditions

In this paper, the nonlinear Schrödinger equation is studied numerically in a symmetric, finite interval $\mathcal{D}=[-L, L]$ subject to the following homogeneous boundary conditions

$$u(-L, t) + \gamma u_x(-L, t) = 0, \quad u(L, t) + \gamma u_x(L, t) = 0 \quad \text{and} \quad t \geq 0. \quad (22)$$

The values $\gamma=0$ and ∞ correspond to Dirichlet and Neumann boundary conditions, respectively.

Since the nonlinear Schrödinger equation and the homogeneous Dirichlet and Neumann boundary conditions are invariant under mirror reflections in x , their respective initial-boundary-value problems also exhibit this invariance; as a consequence, the interaction of a soliton with the left boundary is identical to that with the right boundary. This symmetry or invariance is lost if γ is finite and different from zero, i.e., if homogeneous Robin boundary conditions apply at both boundaries. In this paper, mixed boundary conditions corresponding to $\gamma=1$ are considered, and the results for the Dirichlet, Neumann and Robin boundary conditions are compared with those for both the initial-value problem and the periodic boundary conditions

$$\frac{\partial^n u}{\partial x^n}(x, t) = \frac{\partial^n u}{\partial x^n}(x+2kL, t), \quad \forall n \geq 0, \quad k \in \mathbf{Z}, \quad \mathbf{x} \in \mathcal{D} \equiv [-\mathbf{L}, \mathbf{L}], \quad \mathbf{t} \geq \mathbf{0}. \quad (23)$$

4 Relationships between the Quantum Momentum and Energy Densities

The most important invariants of the initial-value problem of the nonlinear Schrödinger equation are the first, second and third ones. The first, known as wave mass or ‘number of particles’, is

$$\int_{\mathcal{D}} |u|^2 dx, \quad (24)$$

whose integrand will be denoted by ρ_{I1} . The second invariant represents the total momentum in the Hamiltonian formalism and is given by

$$\int_{\mathcal{D}} i (u^* u_x - u u_x^*) dx \quad (25)$$

and whose integrand will be referred to as ρ_{I2} . The third invariant is the total energy or Hamiltonian, i.e.,

$$\int_{\mathcal{D}} \left(|u_x|^2 - \frac{1}{2}|u|^4 \right) dx \quad (26)$$

whose integrand is the Hamiltonian density of the nonlinear Schrödinger equation and will be denoted by ρ_{I3} .

The real and imaginary parts of the quantum momentum density are

$$\mathcal{R}e\{p(x, t)\} = p_R = -\frac{i}{2} (u^* u_x - u u_x^*) \quad (27)$$

$$\mathcal{I}m\{p(x, t)\} = p_I = -\frac{1}{2} (u^* u_x + u u_x^*) \quad (28)$$

those of the kinetic energy density

$$\mathcal{R}e\{e_k(x, t)\} = e_R = -\frac{1}{2} (u^* u_{xx} + u u_{xx}^*) \quad (29)$$

$$\mathcal{I}m\{e_k(x, t)\} = e_I = \frac{i}{2} (u^* u_{xx} - u u_{xx}^*) \quad (30)$$

and those of the diffraction force density

$$\mathcal{R}e\{f_d(x, t)\} = f_R = \frac{1}{2} \frac{\partial}{\partial x} (u^* u_{xx} + u u_{xx}^*) \quad (31)$$

$$\mathcal{I}m\{f_d(x, t)\} = f_I = -\frac{i}{2} \frac{\partial}{\partial x} (u^* u_{xx} - u u_{xx}^*) \quad (32)$$

From the above equations, the following relations may be easily deduced

$$\frac{\partial}{\partial t} \rho_{I1} = -2 \frac{\partial p_R}{\partial x} = \frac{\partial \rho_{I2}}{\partial x}, \quad p_I = -\frac{1}{2} \frac{\partial}{\partial x} \rho_{I1}. \quad (33)$$

It can also be easily shown using the nonlinear Schrödinger equation that the following equations hold

$$\frac{\partial p_R}{\partial t} = -\frac{\partial \rho_{I3}}{\partial x} + f_R, \quad \frac{\partial p_I}{\partial t} = f_I, \quad (34)$$

$$\frac{\partial p}{\partial t} = -\frac{\partial \rho_{I3}}{\partial x} - \frac{\partial e_k}{\partial x}, \quad \frac{\partial \rho_{I3}}{\partial t} = \frac{\partial}{\partial x}(u_x^* u_t + u_x u_t^*) \quad (35)$$

For initial-value problems, i.e., $\mathcal{D} = (-\infty, \infty)$ subject to $|u| \rightarrow 0$ as $|x| \rightarrow \infty$, the above equations imply that the total mass or number of particles, the total momentum in the Hamiltonian formalism and the total energy are invariant. Furthermore,

$$\int_{\mathcal{D}} p \, dx = 0, \quad (36)$$

i.e., the total quantum momentum is zero.

For quarter-plane or semi-infinite, initial-boundary-value problems, i.e., $\mathcal{D} = [0, \infty)$ subject to $|u| \rightarrow 0$ as $x \rightarrow \infty$, the total number of particles is constant for homogeneous Dirichlet or homogeneous Neumann boundary conditions at $x = 0$, and the imaginary part of the total quantum momentum is only zero for homogeneous Dirichlet boundary conditions at $x = 0$, whereas both the total quantum momentum and its real part are different from zero.

For the finite-line, initial-boundary-value problems considered in Section 3, the total number of particles is constant for homogeneous Dirichlet or homogeneous Neumann boundary conditions at both boundaries; the imaginary part of the total quantum momentum is zero for periodic or for homogeneous Dirichlet boundary conditions at both boundaries. The total quantum momentum and its real part are different from zero.

5 Numerical Method

The Crank-Nicolson method was used to discretize Eq. (10) in the interval $[-L, L]$, and a Newton-Raphson technique was employed to solve the resulting system of nonlinear algebraic equations. The diagonally dominant,

tridiagonal system of linear algebraic equations that result from the Newton-Raphson method was solved by means of a 2×2 block-oriented version of the Thomas algorithm. In the periodic case, a natural optimization of the Gaussian elimination technique for periodic problems that yields quasi-tridiagonal systems has been used before applying the Thomas algorithm [12].

The Crank-Nicolson method is conservative since it preserves a discrete equivalent of the first invariant, cf. Eq. (24), i.e., the L^2 norm of the solution, for the discrete, initial-value problem, and for the two-point initial-value problem with periodic or Dirichlet boundary conditions.

The evaluation of the high-order derivatives of the soliton amplitude required for the calculation of the soliton energy and force densities was performed so as to preserve both the maximum possible symmetry in the finite difference operators and second-order accuracy. It should be noted that, in the periodic case, symmetric, second-order accurate in space, stencils were employed at all the spatial grid points, while, for the Dirichlet, Neumann and Robin boundary conditions, asymmetric stencils were introduced near the boundary points in order to avoid the use of fictitious points.

6 Presentation of Results

In this section, some sample results (cf. Figs. 1–5) that illustrate the nonlinear force density, the real part of the diffraction force density, the total force density, i.e., the sum of the nonlinear force density and the real part of the diffraction force density, and the real part of the momentum density are presented as functions of space and time for the four types of boundary

conditions considered in this paper. Figures 1–5 also show the space-time isocontours of the three-dimensional data presented in these figures. The results presented in Figs. 1–5 as well as in Figs. 6–10 correspond to an interval of $L=50$, $A=c=1$, $x_0=\phi_0=0$, and spatial and temporal step sizes equal to 0.25 and 0.01, respectively.

Figure 1 corresponds to periodic boundary conditions and shows that the nonlinear force density has an S -shape which is nearly the mirror reflection of that for the diffraction force density. The total force density has also an S -shape similar to the nonlinear one which indicates that, for periodic boundary conditions, the nonlinear force density is larger than the diffraction one. The momentum density has a bell-shape similar to that of the soliton amplitude.

Figure 2 illustrates the large changes in the magnitude of the force densities introduced by homogeneous Dirichlet boundary conditions and, especially, in the collision of the soliton with the right boundary. It is interesting to note that the shape of the nonlinear force density prior to and after the collision of the soliton with the right boundary is the same owing to the symmetry of the nonlinear Schrödinger equation and boundary conditions; however, its magnitude increases greatly in the collision process because the amplitude of the soliton at the boundary is zero. Figure 2 also shows that the nonlinear force density is larger than the diffraction one, and that the momentum density changes sign once the soliton rebounds from the right boundary. Note that the Dirichlet boundary conditions require that the momentum density at the boundary be zero; therefore, the change in the momentum is smooth and the change in its sign is associated with the different directions of the soliton velocity prior to the collision and after the

soliton rebounds from the boundary.

Figure 3 corresponds to homogeneous Neumann boundary conditions and illustrates the S -shapes of the nonlinear, diffraction and total force densities prior to and after the collision of the soliton with the right boundary; this collision is accompanied by large increases in the magnitudes of these densities. During the collision, the nonlinear force density shows a relative maximum near to the right boundary, whereas the diffraction and total force densities exhibit extrema. Figure 3 also indicates that, during the collision with the right boundary, the diffraction force exceeds the magnitude of the nonlinear one at the boundary, whereas the latter is larger than the former near to, but away from, the boundary. The momentum density shown in Figure 3 changes sign upon the collision of the soliton with the boundary, and its value at the boundary is zero.

Comparisons amongst the momentum densities for the periodic, Dirichlet and Neumann boundary conditions indicate that the soliton penetrates into the boundary in the periodic and Neumann cases, i.e., $u(L, t) \neq 0$, whereas it does not penetrate into the boundary for the Dirichlet case; the momentum preserves its sign in the periodic case owing to the transparency of the boundary and has the same shape for the Dirichlet and Neumann boundary conditions.

Since the nonlinear Schrödinger equation with Robin boundary conditions is not a symmetric problem, the interaction of a soliton with the left boundary is expected to be different from that with the right one. For this reason, the soliton interactions with both boundaries must be considered as shown in Figures 4 and 5 which correspond to the first and second collisions, i.e.,

a collision with the right boundary followed by another one with the left boundary. Figure 4 indicates the S -shapes of the nonlinear, diffraction and total force densities prior to and after the collision of the soliton with the right boundary. The nonlinear force density exhibits a relative maximum and a relative minimum near to, but away from, the boundary where its value is not zero. Similar trends are observed in the diffraction force density until its relative maximum becomes an extremum at the boundary. Figure 4 also shows that the nonlinear force is greater than the diffraction one except very near to the boundary during the collision process. The momentum density presented in Figure 4 has the same shape as those for the Dirichlet and Neumann boundary conditions, except that its value at the right boundary is different from zero.

Figure 5 indicates the lack of symmetry of the nonlinear Schrödinger equation subject to Robin boundary conditions. In particular, the nonlinear force density maintains its S -shape prior to and after the collision of the soliton with the left boundary; however, compared with the collision with the right boundary, this density exhibits a plateau before reaching a negative extremum at the boundary. Figure 5 also shows that the diffraction force preserves its S -shape prior to and after the collision of the soliton with the left boundary, and that it exhibits a plateau near to and a positive extremum at the left boundary. The total force density indicates that the nonlinear force is larger than the diffraction one, while the momentum changes sign upon the collision of the soliton with the left boundary. The isocontours presented in Figures 4 and 5 indicate that the soliton becomes closer to the right boundary than to the left one.

In Figures 6–10, the negative values of the kinetic, potential and total energy, and of the momentum are presented as functions of time. Note that these quantities are the integrals, from the left to the right boundary, of their corresponding densities, that the kinetic energy has been calculated from the real part of its density, and that the momentum has been obtained from the absolute value of its density.

The results presented in Figure 6 indicate that the kinetic and potential energies are nearly constant and have opposite signs for the two-point, periodic, initial-value problem. The total energy, i.e., the sum of the potential and kinetic energies, is almost constant except for a minimum at about $t=50$ which corresponds to the time at which the soliton crosses the boundary. The momentum presented in Figure 6 is also nearly constant.

Figure 7 corresponds to Dirichlet boundary conditions and shows that the kinetic energy is larger than the potential one which is negative; the total energy is positive and exhibits a maximum at about $t=50$ which corresponds to the collision of the soliton with the right boundary. The results presented in Figure 7 clearly indicate that the collision of the soliton with a Dirichlet boundary is accompanied by an increase (decrease) in energy as the soliton approaches (rebounds from) the boundary, and that the energies after rebound are the same as those prior to the collision. The momentum presented in Figure 7 indicates the deceleration (acceleration) of the soliton as it approaches (recedes from) the right boundary; however, these deceleration and acceleration processes do not cause large variations in the soliton momentum.

The results presented in Figure 8 correspond to Neumann boundary con-

ditions and exhibit similar trends to those presented in Figure 7 except for the small, relative minima that surround the relative maxima of the kinetic, potential and total energies. Figure 8 also shows that the collision of the soliton with a Neumann boundary produces larger increases in energy in smaller intervals of time than that with a Dirichlet boundary. Large increases are also observed in the momentum as the soliton collides with the right boundary. However, both the energies and the momentum recover their values prior to the collision after the soliton rebounding process is completed.

The energies presented in Figures 9 and 10 correspond to the first collision of the soliton with the right and left boundaries, respectively, for the Robin boundary conditions, and exhibit the same trends as, but have smaller magnitude than, those corresponding to the Neumann boundary conditions presented in Figure 8; the duration of the soliton interaction with the boundaries is shorter (longer) than those of the Dirichlet (Neumann) boundary conditions presented in Figure 7 (8). The most noteworthy features of the results presented in Figures 9 and 10 are the increase in the background radiation as the soliton collides with the left boundary, the decrease (increase) in the momentum as the soliton collides with the right (left) boundary, and the relative maxima and minimum observed in the momentum upon the collision of the soliton with the left boundary.

7 Conclusions

A quantum mechanics analogy is used to determine the forces on and the energies of solitons governed by the nonlinear Schrödinger equation subject

to periodic and to homogeneous Dirichlet, Neumann and Robin boundary conditions in finite intervals. For all the boundary conditions considered in this paper, it has been shown that the the nonlinear, diffraction and total force densities have S -shape profiles and increase in magnitude as the soliton interacts with the boundaries. This interaction is characterized by an increase in the force densities; the largest increase corresponds to the homogeneous Neumann boundary conditions.

The values of the force and energy densities after the soliton rebound from the boundary is completed, are same values as those prior to the interaction with of the soliton with the boundary, and, except during the collision process, the nonlinear force density is larger than the diffraction one. During the collision process, the nonlinear force is larger than the diffraction one for the Dirichlet boundary conditions; the former is smaller than the latter at the boundary for the Neumann conditions.

The lack of symmetry of the Robin boundary conditions has been illustrated by the different dynamics of the soliton collisions with the right and left boundaries. In the collision with the right (left) boundary, the magnitude of the diffraction (nonlinear) density force at the boundary is larger (smaller) than the nonlinear (diffraction) one, and the soliton becomes closer to the right than to the left boundary. Since the nonlinear force is larger than the diffraction one when the soliton is sufficiently far away from the boundaries, it may be concluded that self-focusing effects are more important as regard the quantum mechanics analogy developed in this paper.

The kinetic, potential and total energies of the soliton decrease as the softness of the boundary conditions is increased, i.e., they are largest (small-

est) for Neumann (Dirichlet) boundary conditions, and are nearly constant for the periodic boundary conditions.

Acknowledgments

This research was supported by the Spanish D.G.I.C.Y.T. under Project no. PB91-0767. The second author (F.R.V.) has a fellowship from the Programa Sectorial de Formación de Profesorado Universitario y Personal Investigador, Subprograma de Formación de Investigadores "Promoción General del Conocimiento", from the Ministerio de Educación y Ciencia of Spain.

References

- [1] M. J. Ablowitz and H. Segur, *Solitons and the Inverse Scattering Transform*, SIAM, Philadelphia (1981).
- [2] G. L. Lamb, *Elements of Soliton Theory*, John Wiley & Sons, New York (1980).
- [3] C. K. Chu and R. L. Chou, Solitons Induced by Boundary Conditions, In *Advances in Applied Mechanics*, (Edited by J. W. Hutchinson and T. Y. Wu), *Academic Press, New York* vol. 27, pp. 283-302 (1990).
- [4] D. J. Kaup and P. J. Hansen, The Forced Nonlinear Schrödinger Equation, *Physica D* **18**, 77-84 (1986).

- [5] R. F. Bikbaev and V. O. Tarasov, Initial Boundary Value Problem for the Nonlinear Schrödinger Equation, *J. Phys. A: Math. Gen.* **24**, 2507–2516 (1991).
- [6] A. S. Fokas, An Initial-Boundary Value Problem for the Nonlinear Schrödinger Equation, *Physica D* **35**, 167–185 (1989).
- [7] M. J. Ablowitz and H. Segur, The Inverse Scattering Transform: the Semi-Infinite Interval, *J. Math. Phys.* **16**(5) 1054–1056 (1975).
- [8] D. J. Kaup, Forced Integrable Systems — An Overview, In *Nonlinear Systems of Partial Differential Equations in Applied Mathematics, Part 1*, Proceedings of the SIAM-AMS Summer Seminar, Santa Fe, New Mexico, (Edited by B. Nicolaenko, D. D. Holm and J. M. Hyman), AMS Lect. Appl. Math., vol. 23, pp. 195–215 (1985).
- [9] D. J. Kaup, Approximations for the Inverse Scattering Transform, In *Dynamical Problems in Soliton Systems*, (Edited by S. Takeno), pp. 12–22, Springer-Verlag, Berlin, (1985).
- [10] J.-R. Bian and A. K. Chan, Computations of the Diffraction Effect and the Nonlinear Effect on Spatial Solitons in Nonlinear Planar Waveguides, *Microwave and Optical Technology Letters* **4**, 184–191 (1991).
- [11] L. D. Landau and E. M. Lifshitz, *Quantum Mechanics (Non-relativistic Theory)*, 3rd. ed., Pergamon Press, New York (1977).
- [12] T. R. Taha and M. J. Ablowitz, Analytical and Numerical Aspects of Certain Nonlinear Evolution Equations. II. Numerical, Nonlinear Schrödinger Equation, *J. Comp. Phys.* **55**, 203–230 (1984).

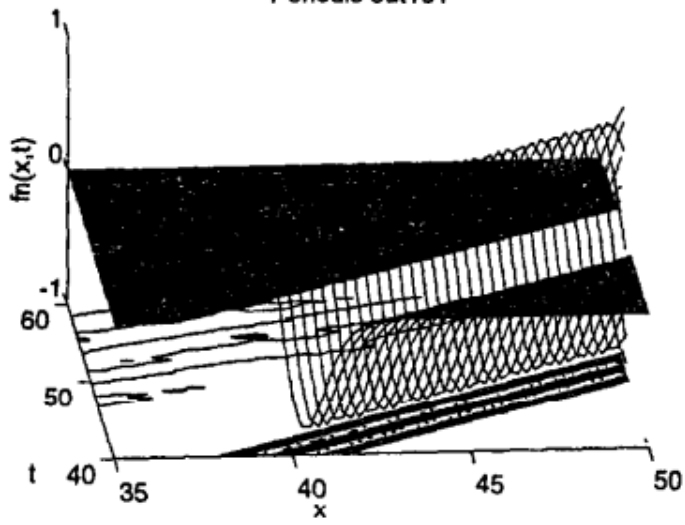
- [13] V. E. Zakharov and A. B. Shabat, Exact Theory of Two-Dimensional Self-Focusing and One-Dimensional Self-Modulation of Waves in Nonlinear Media, *Sov. Phys. JETP* **34**(1) 62–69 (1972).
- [14] J. P. Gordon, Interaction Forces Among Solitons in Optical Fibers, *Optics Lett.* **8**(11) 596–598 (1983).

Figure Captions

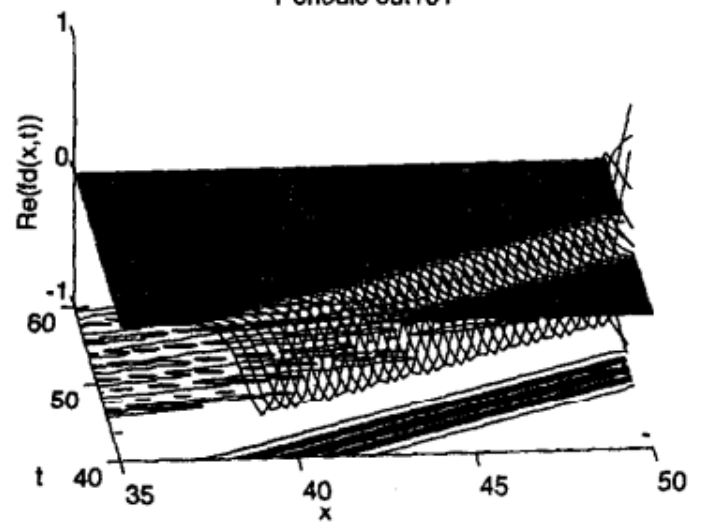
1. Nonlinear (f_n), diffraction ($\text{Re}(f_d)$) and total (f_{total}) force densities and momentum density (p) for periodic boundary conditions.
2. Nonlinear (f_n), diffraction ($\text{Re}(f_d)$) and total (f_{total}) force densities and momentum density (p) for Dirichlet boundary conditions.
3. Nonlinear (f_n), diffraction ($\text{Re}(f_d)$) and total (f_{total}) force densities and momentum density (p) for Neumann boundary conditions.
4. Nonlinear (f_n), diffraction ($\text{Re}(f_d)$) and total (f_{total}) force densities and momentum density (p) for Robin boundary conditions and first collision with the right boundary.
5. Nonlinear (f_n), diffraction ($\text{Re}(f_d)$) and total (f_{total}) force densities and momentum density (p) for Robin boundary conditions and first collision with the left boundary.
6. Kinetic, potential and total energy, and momentum for periodic boundary conditions.
7. Kinetic, potential and total energy, and momentum for Dirichlet boundary conditions.
8. Kinetic, potential and total energy, and momentum for Neumann boundary conditions.
9. Kinetic, potential and total energy, and momentum for Robin boundary conditions and first collision with the right boundary.

10. Kinetic, potential and total energy, and momentum for Robin boundary conditions and first collision with the left boundary.

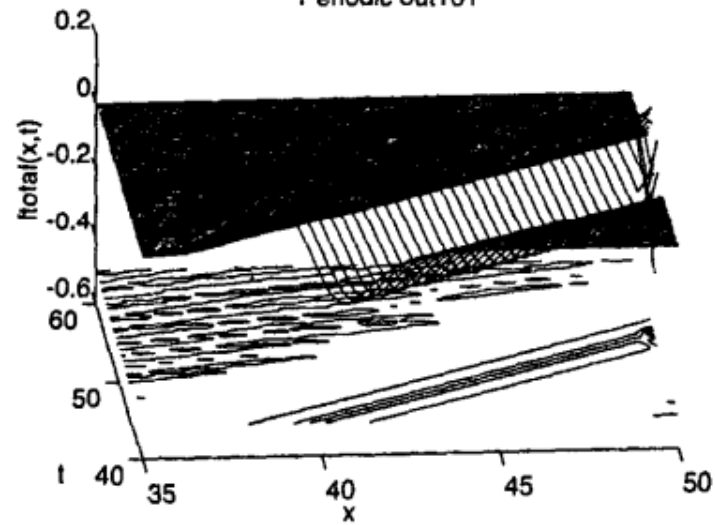
Periodic out101



Periodic out101



Periodic out101



Periodic out101

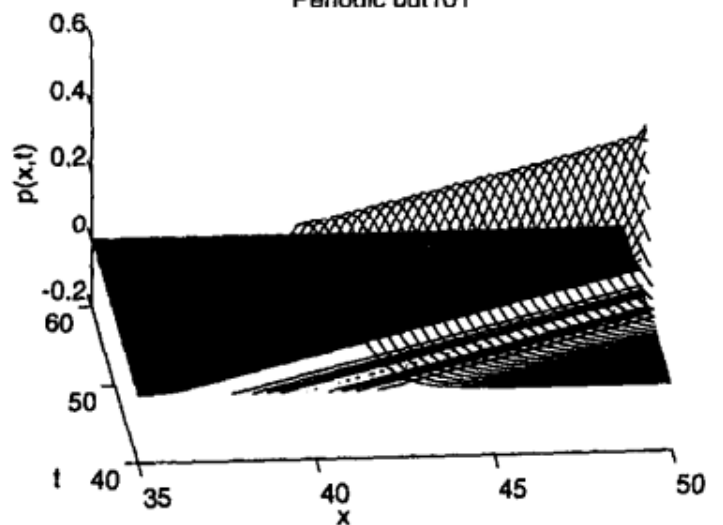
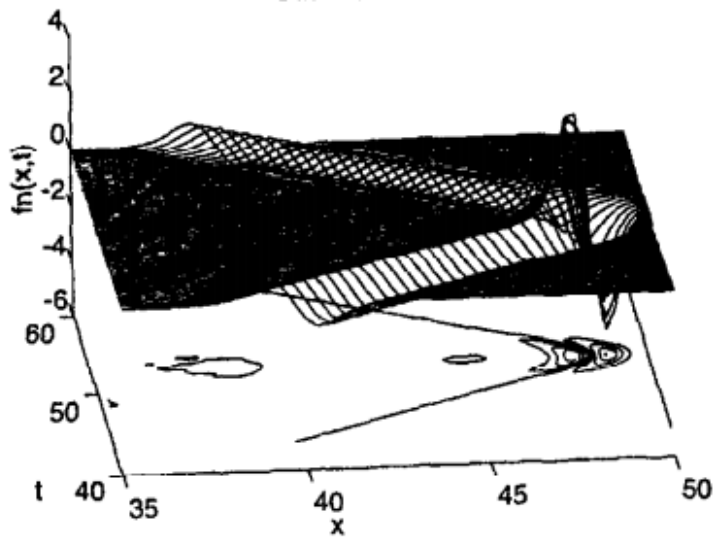
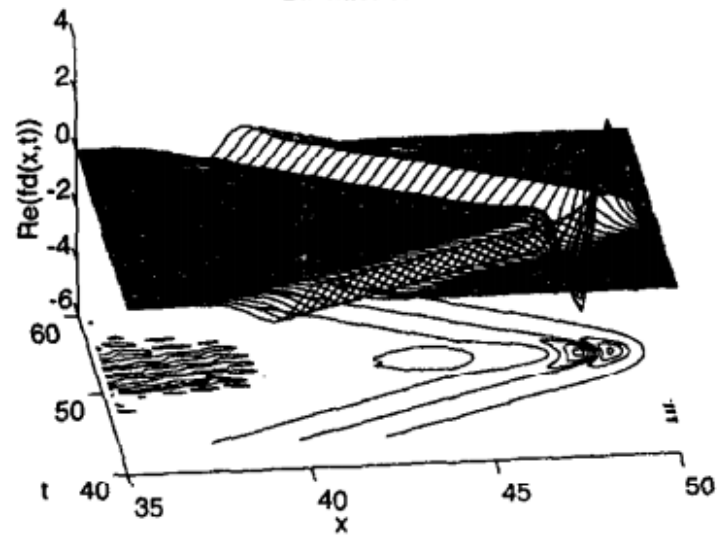


Figure 1. Nonlinear (f_n), diffraction ($\text{Re}(f_d)$) and total (f -total) force densities and momentum density (p) for periodic boundary conditions.

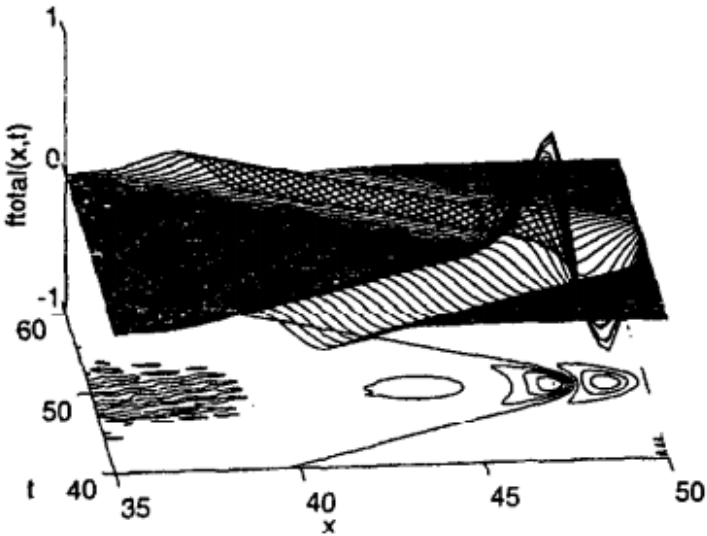
Dirichlet out301



Dirichlet out301



Dirichlet out301



Dirichlet out301

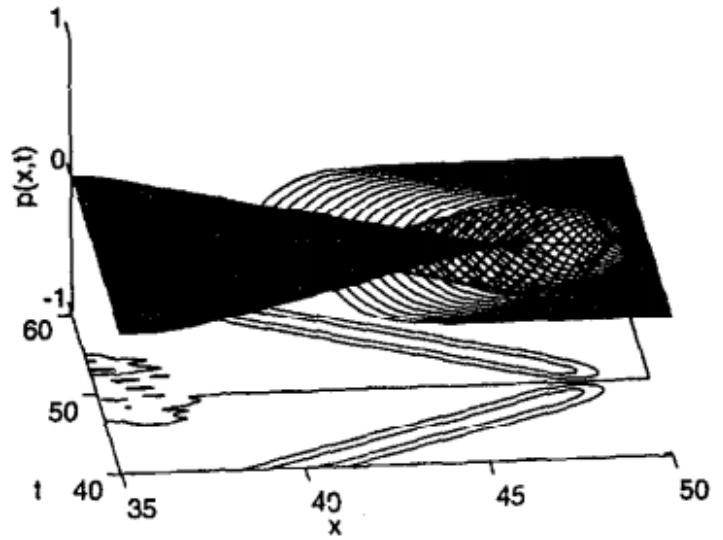
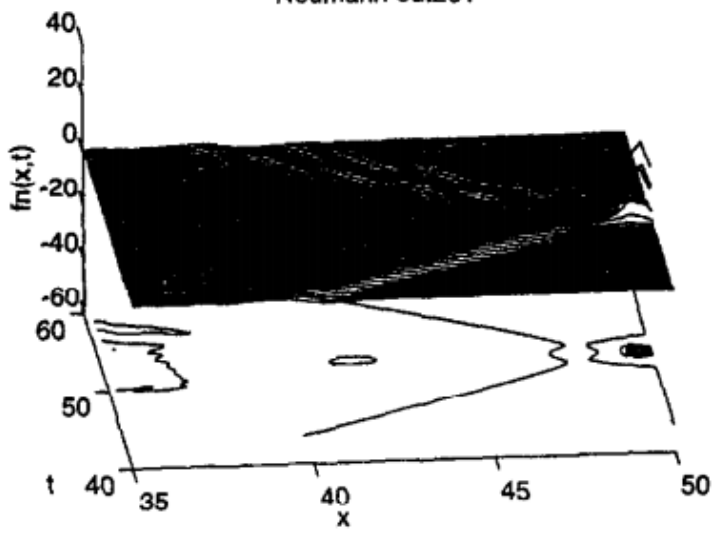
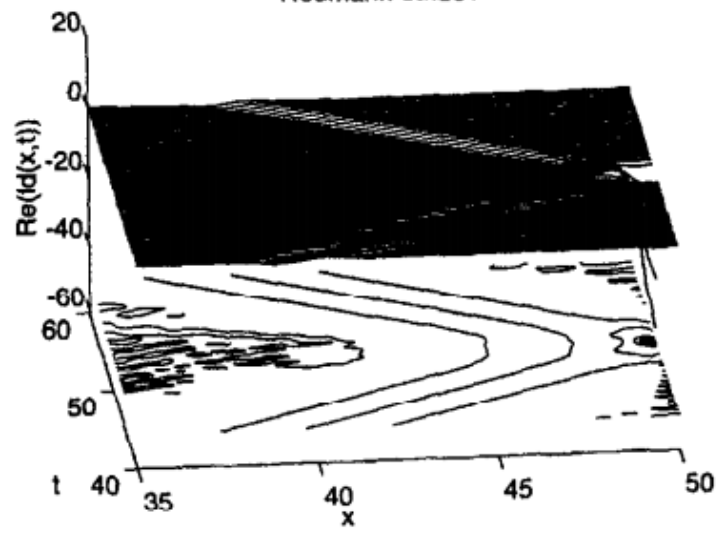


Figure 2. Nonlinear (f_n), diffraction ($\text{Re}(f_d)$) and total (f -total) force densities and momentum density (p) for Dirichlet boundary conditions.

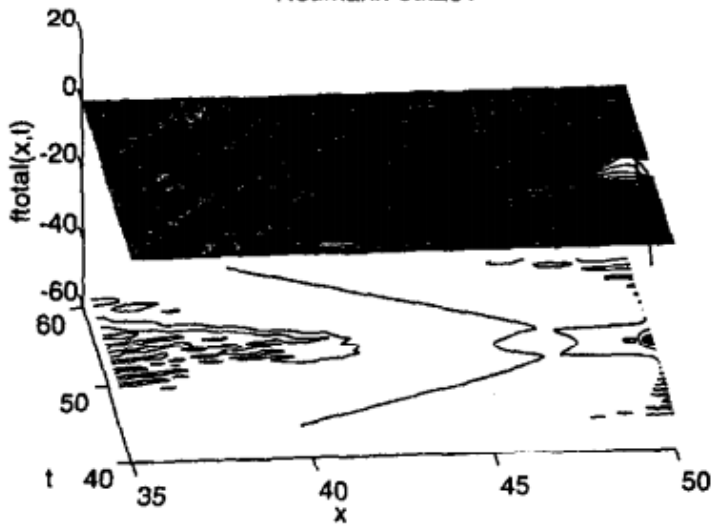
Neumann out201



Neumann out201



Neumann out201



Neumann out201

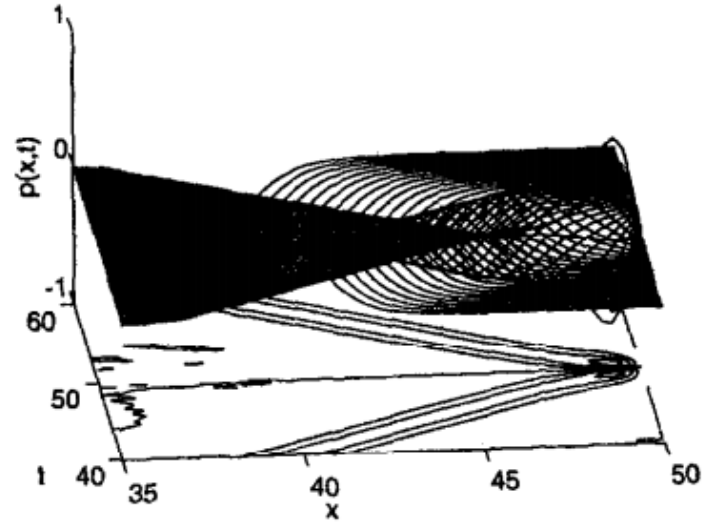
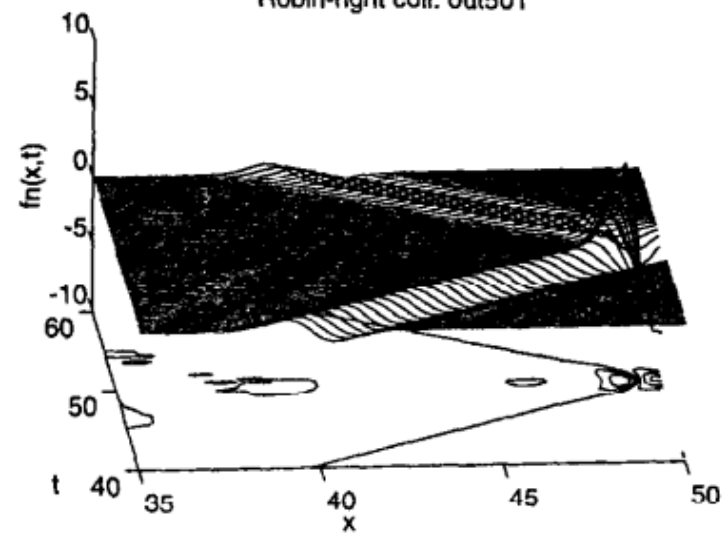
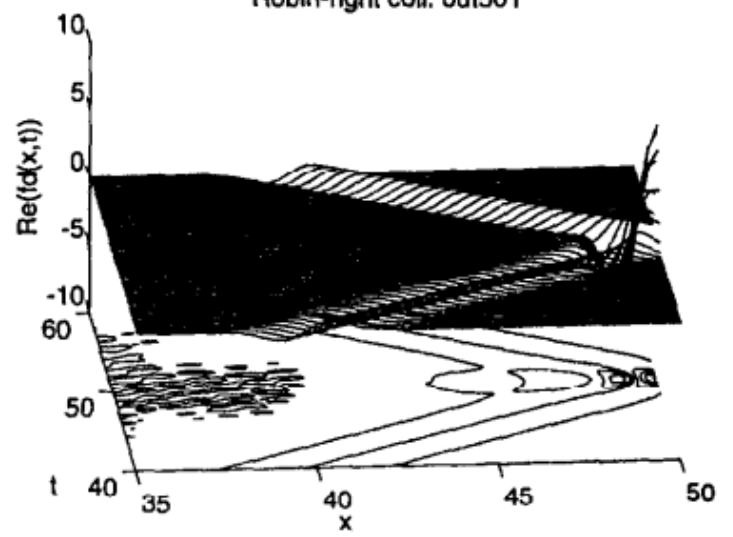


Figure 3. Nonlinear (f_n), diffraction ($\text{Re}(f_d)$) and total (f -total) force densities and momentum density (p) for Neumann boundary conditions.

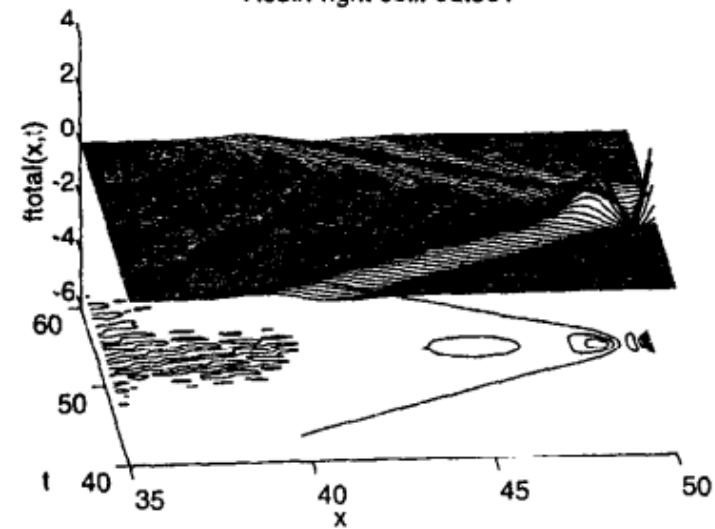
Robin-right coll. out501



Robin-right coll. out501



Robin-right coll. out501



Robin-right coll. out501

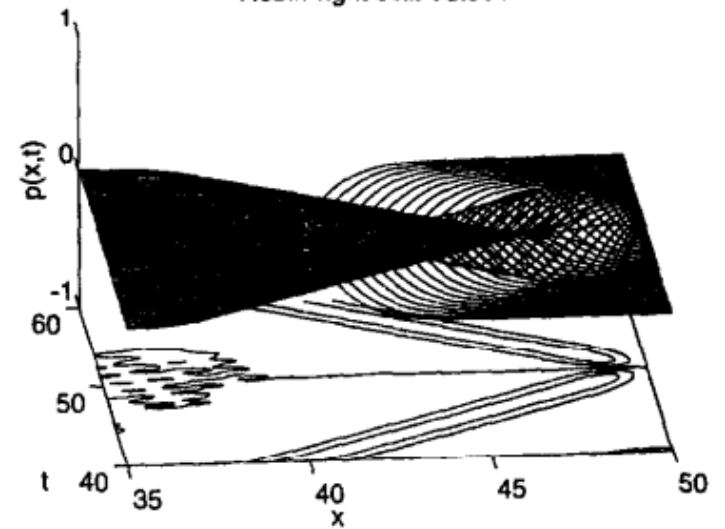


Figure 4. Nonlinear (f_n), diffraction ($\text{Re}(f_d)$) and total (f -total) force densities and momentum density (p) for Robin boundary conditions and first collision with the right boundary.

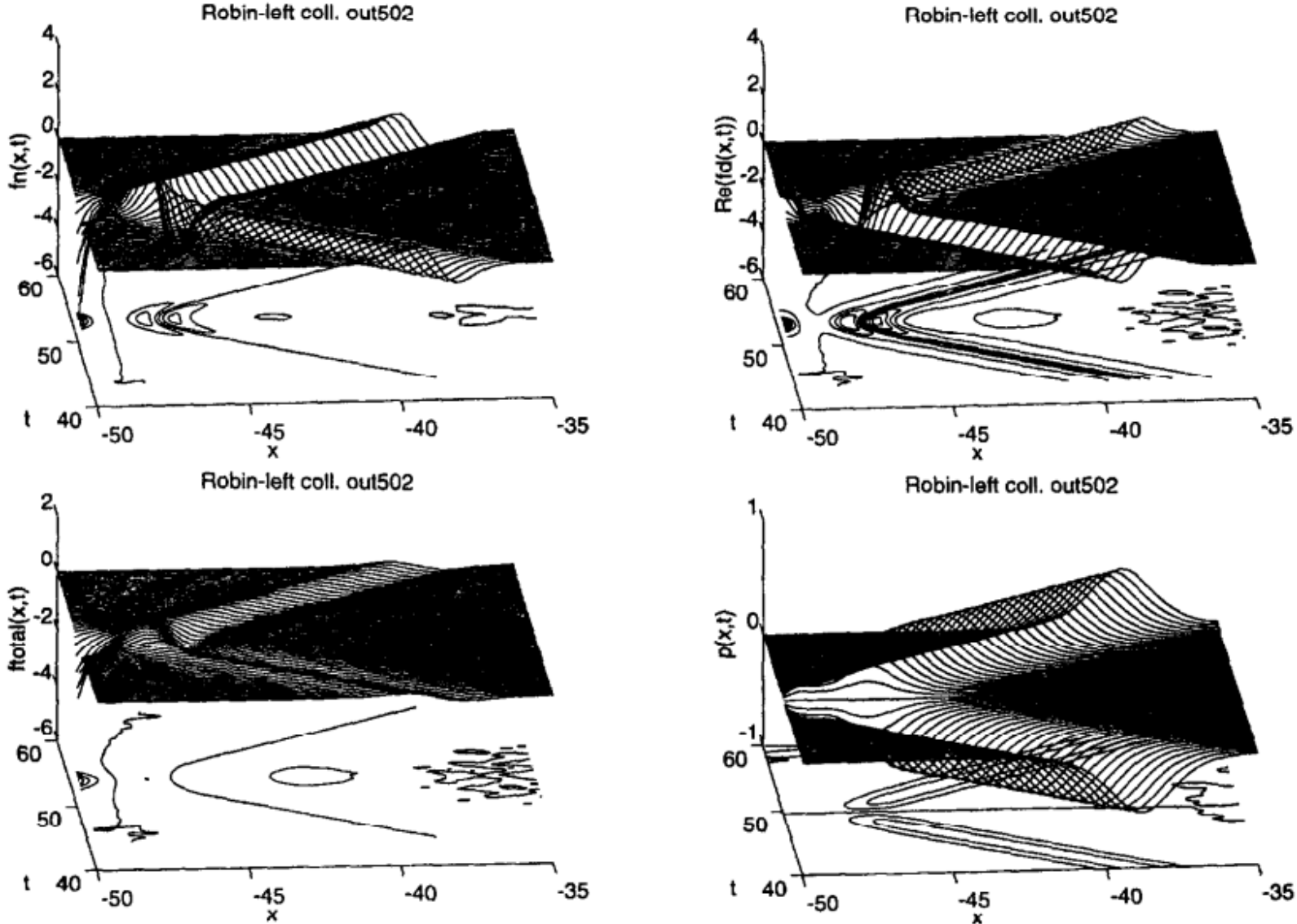


Figure 5. Nonlinear (f_n), diffraction ($\text{Re}(f_d)$) and total (f -total) force densities and momentum density (p) for Robin boundary conditions and first collision with the left boundary.

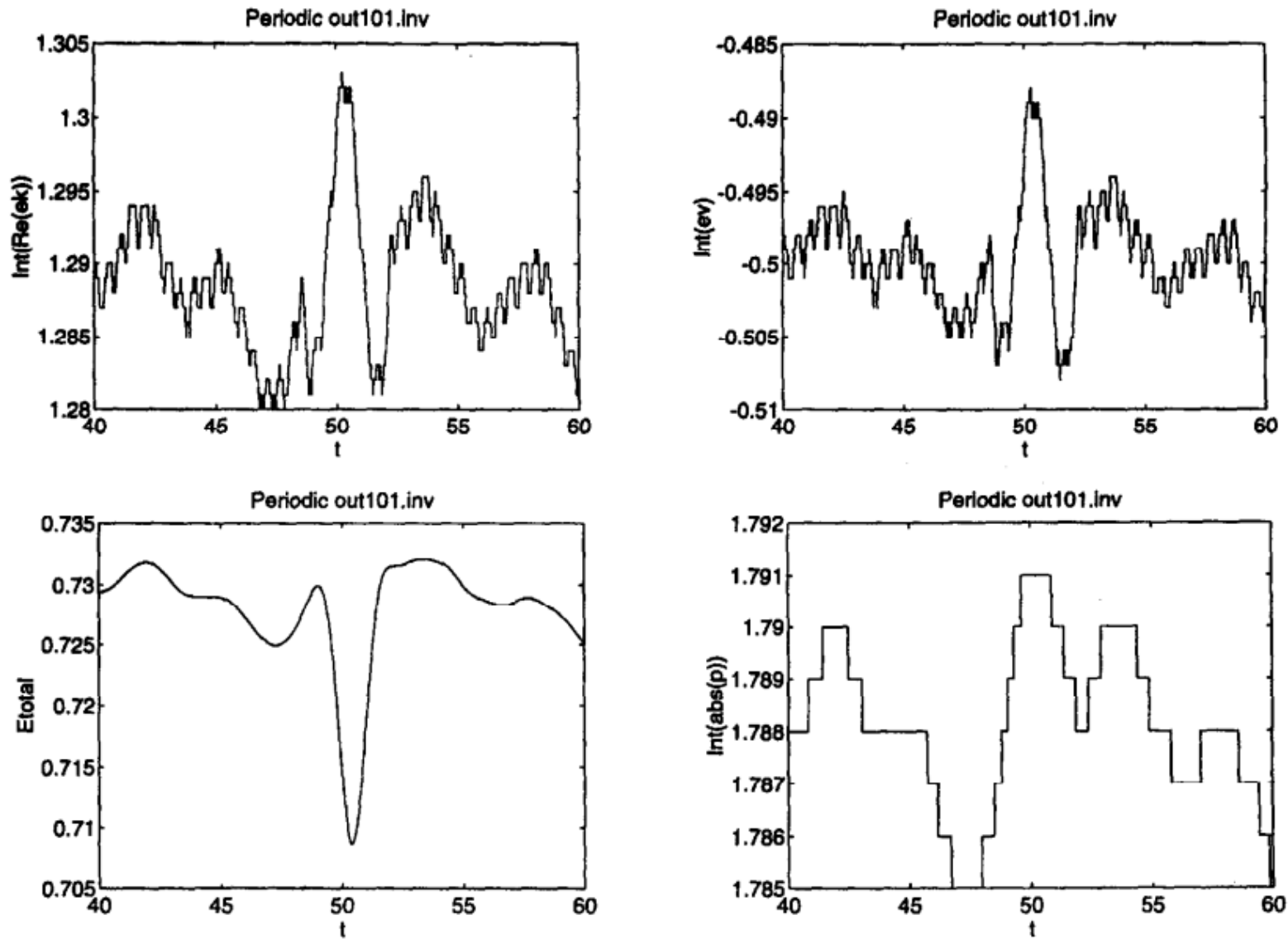
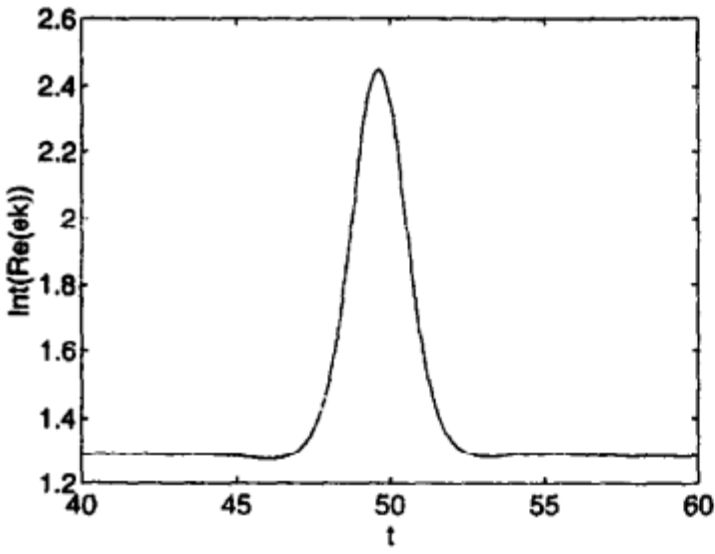
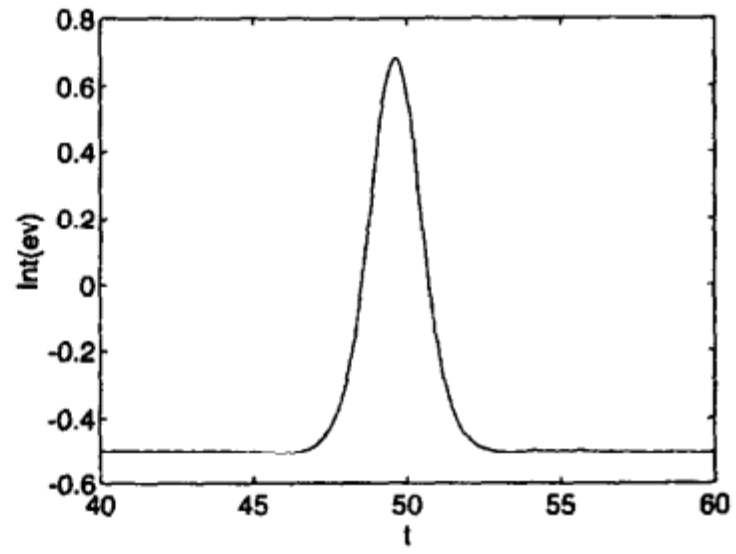


Figure 6. Kinetic, potential and total energy, and momentum for periodic boundary conditions.

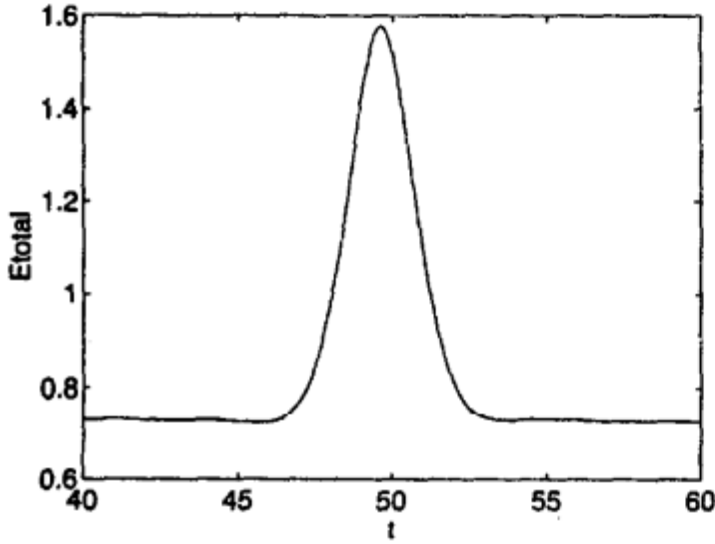
Dirichlet out301.inv



Dirichlet out301.inv



Dirichlet out301.inv



Dirichlet out301.inv

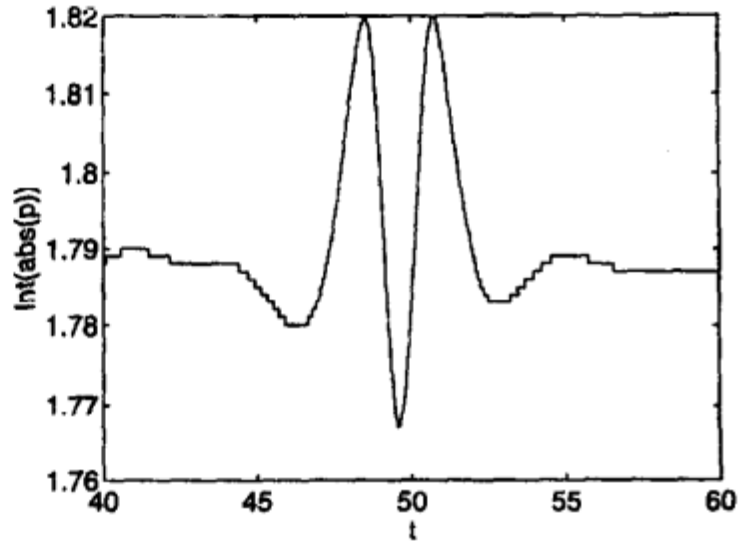
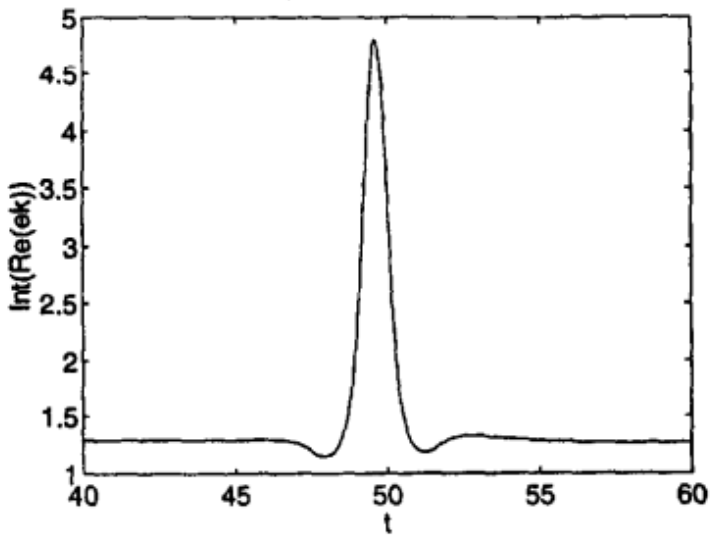
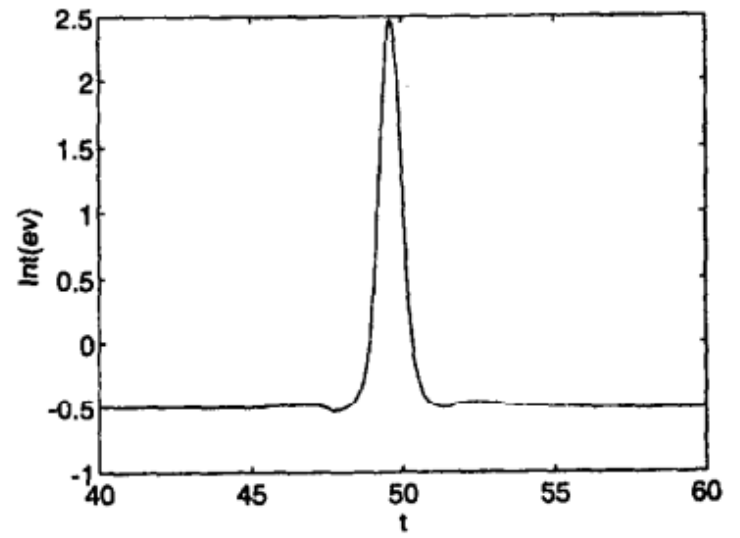


Figure 7. Kinetic, potential and total energy, and momentum for Dirichlet boundary conditions.

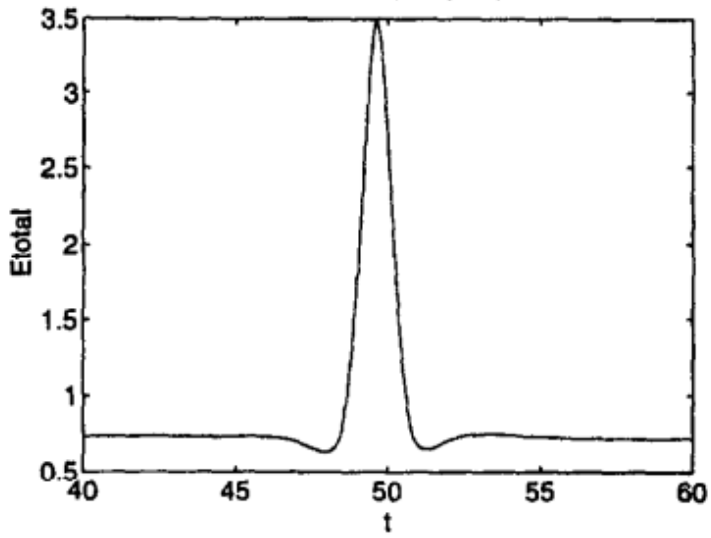
Neumann out201.inv



Neumann out201.inv



Neumann out201.inv



Neumann out201.inv

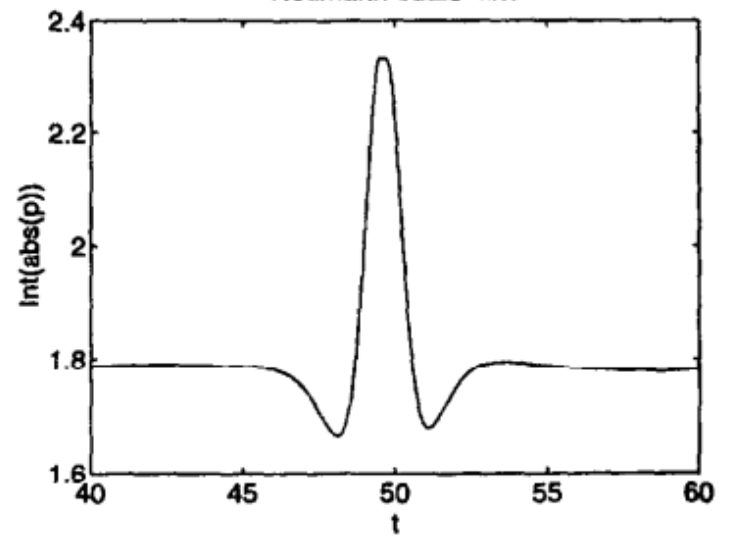


Figure 8. Kinetic, potential and total energy, and momentum for Neumann boundary conditions.

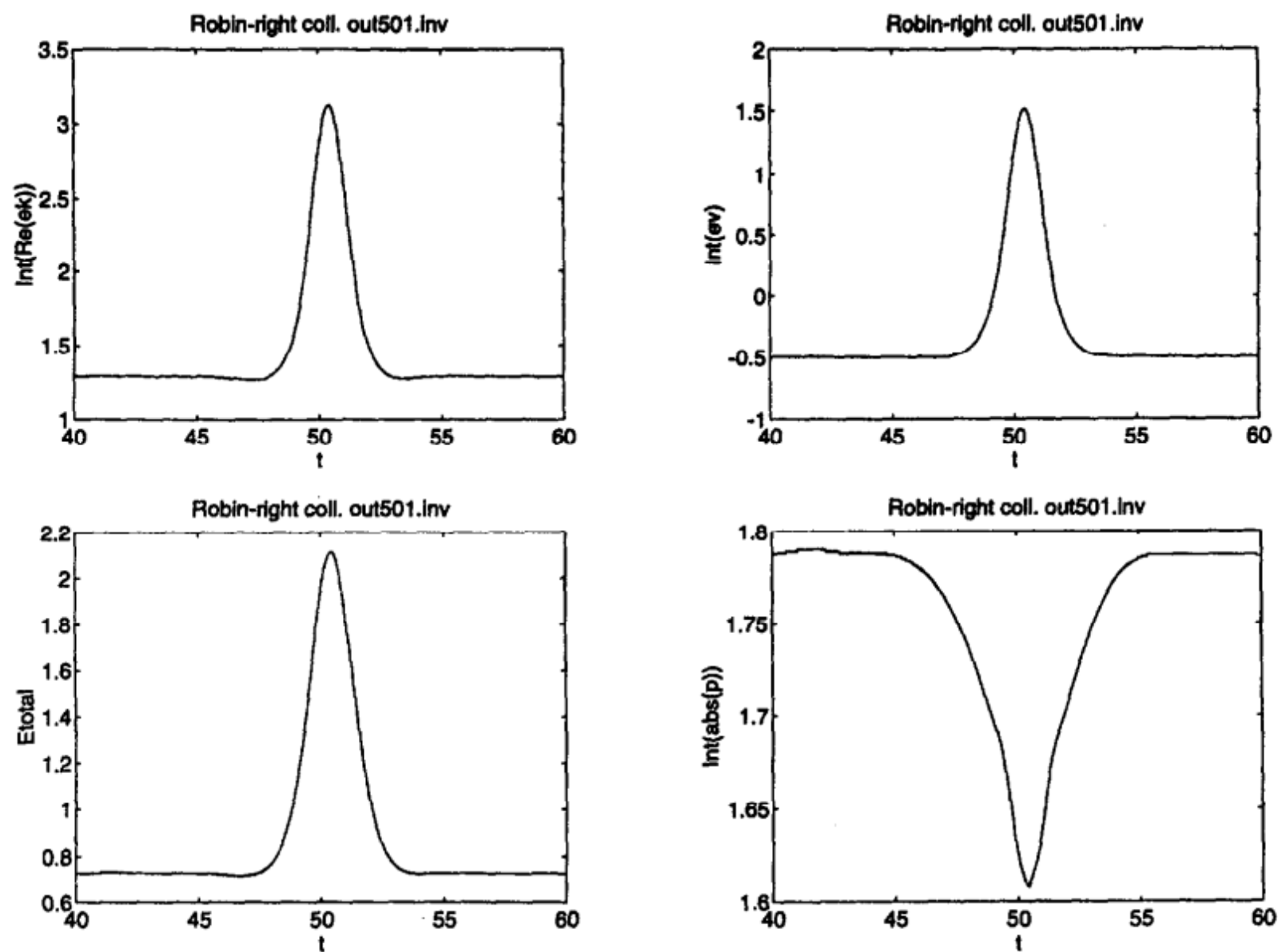


Figure 9. Kinetic, potential and total energy, and momentum for Robin boundary conditions and first collision with the right boundary.

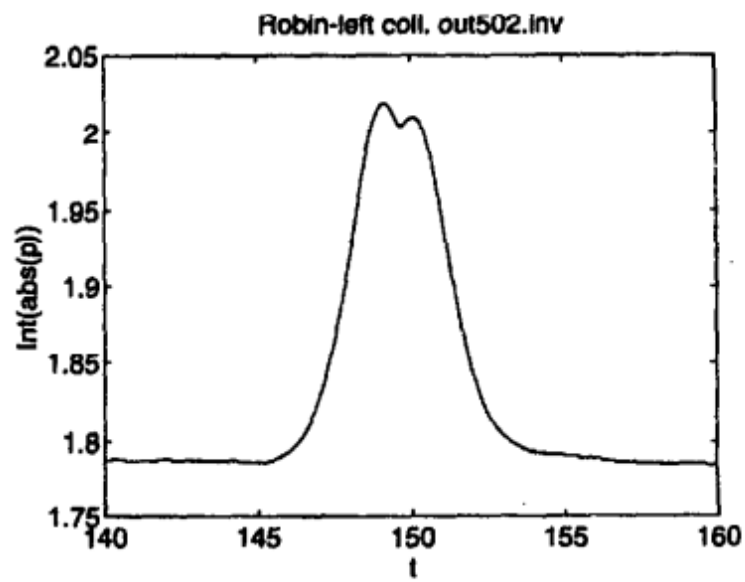
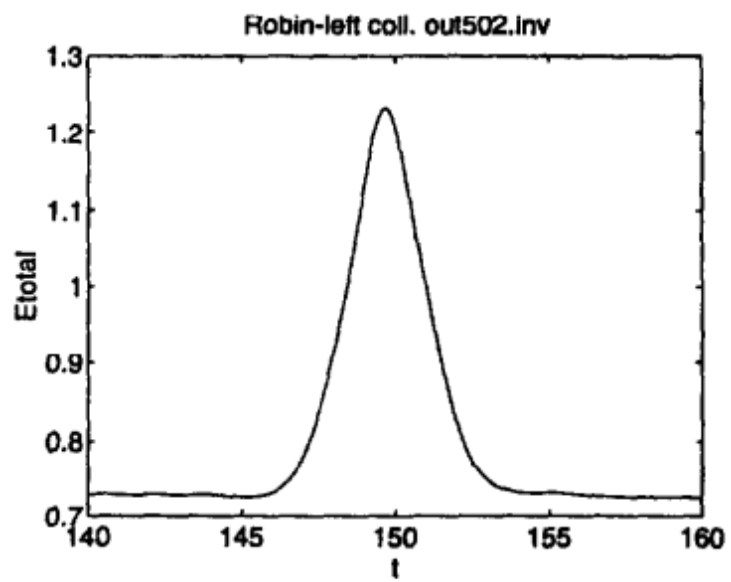
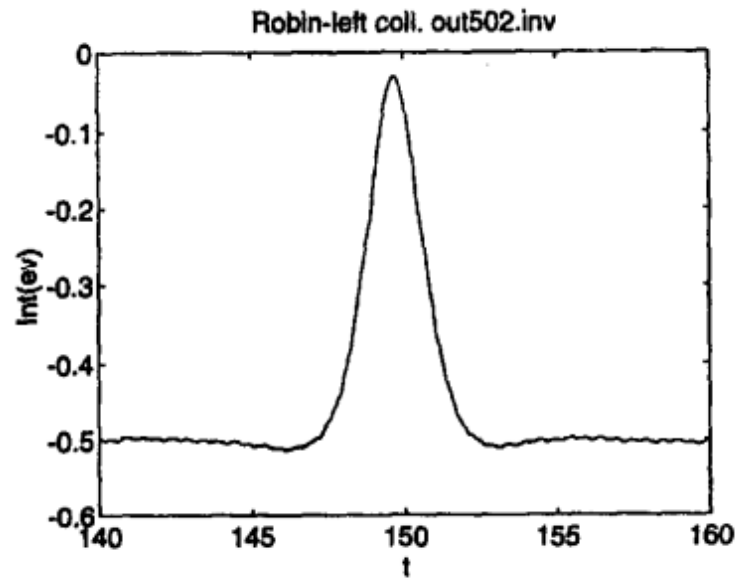
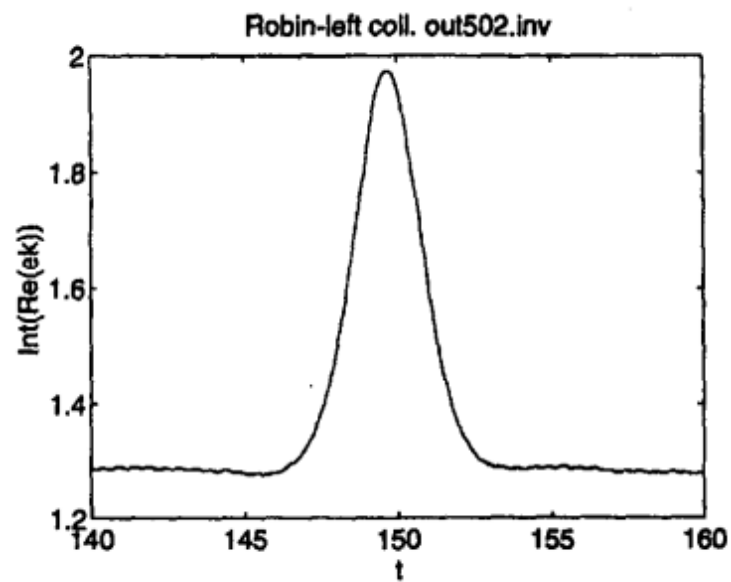


Figure 10. Kinetic, potential and total energy, and momentum for Robin boundary conditions and first collision with the left boundary.